Transplantation of human embryonic stem cell-derived retinal tissue in two primate models of retinal degeneration

Hiroshi Shirai[a,b], Michiko Mandai[a,1], Keizo Matsushita[a,c], Atsushi Kuwahara[c,d,e], Shigenobu Yonemura[f], Tokushige Nakano[d,e], Juthaporn Assawachananont[a], Toru Kimura[c], Koichi Saito[e], Hiroko Terasaki[b], Mototsugu Eiraku[g], Yoshiki Sasai[d], and Masayo Takahashi[a]

[a]Laboratory for Retinal Regeneration, RIKEN Center for Developmental Biology, Chuo, Kobe 650-0047, Japan; [b]Department of Ophthalmology, Nagoya University Graduate School of Medicine, Showa, Nagoya 466-8550, Aichi, Japan; [c]Regenerative and Cellular Medicine Office, Sumitomo Dainippon Pharma Co., Ltd., Chuo, Kobe 650-0047, Japan; [d]Neurogenesis and Organogenesis Group, RIKEN Center for Developmental Biology, Chuo, Kobe 650-0047, Japan; [e]Environmental Health Science Laboratory, Sumitomo Chemical Co., Ltd., Konohana, Osaka 554-8558, Japan; [f]Electron Microscope Laboratory, RIKEN Center for Developmental Biology, Chuo, Kobe 650-0047, Japan; and [g]Laboratory for in Vitro Histogenesis, RIKEN Center for Developmental Biology, Chuo, Kobe 650-0047, Japan

Edited by Donald J. Zack, Johns Hopkins University, Baltimore, MD, and accepted by the Editorial Board November 17, 2015 (received for review June 27, 2015)

Retinal transplantation therapy for retinitis pigmentosa is increasingly of interest due to accumulating evidence of transplantation efficacy from animal studies and development of techniques for the differentiation of human embryonic stem cells (hESCs) and induced pluripotent stem cells into retinal tissues or cells. In this study, we aimed to assess the potential clinical utility of hESC-derived retinal tissues (hESC-retina) using newly developed primate models of retinal degeneration to obtain preparatory information regarding the potential clinical utility of these hESC-retinas in transplantation therapy. hESC-retinas were first transplanted subretinally into nude rats with or without retinal degeneration to confirm their competency as a graft to mature to form highly specified outer segment structure and to integrate after transplantation. Two focal selective photoreceptor degeneration models were then developed in monkeys by subretinal injection of cobalt chloride or 577-nm optically pumped semiconductor laser photocoagulation. The utility of the developed models and a practicality of visual acuity test developed for monkeys were evaluated. Finally, feasibility of hESC-retina transplantation was assessed in the developed monkey models under practical surgical procedure and postoperational examinations. Grafted hESC-retina was observed differentiating into a range of retinal cell types, including rod and cone photoreceptors that developed structured outer nuclear layers after transplantation. Further, immunohistochemical analyses suggested the formation of host–graft synaptic connections. The findings of this study demonstrate the clinical feasibility of hESC-retina transplantation and provide the practical tools for the optimization of transplantation strategies for future clinical applications.

photoreceptors | transplantation | retinal degeneration | primate model | human embryonic stem cells

Retinitis pigmentosa (RP) is a genetic disease characterized by progressive loss of rod photoreceptors, with >45 causal genes reported to date (1). In advanced cases, secondary changes may occur, including cone photoreceptor degeneration and severe visual field loss (2). Therapeutic strategies for RP have largely focused on delaying disease progression (3, 4) but have so far failed to provide clinical therapies with validated efficacy. Studies in gene therapy (5), replacement therapies using artificial prostheses (6), and therapies targeting transmembrane proteins, such as channel rhodopsins (7, 8), are currently in progress. Photoreceptor transplantation has recently emerged as a promising therapeutic option after the demonstration of significant integration of transplanted photoreceptors, with possible synaptic connection and functional restoration, in rodent studies (9–14). Furthermore, the recent development of protocols for the culture of self-organizing optic cups and 3D neural retinas from human embryonic stem cells (hESCs) (15, 16) and human-induced pluripotent stem cells (hiPSCs) (17) has allowed the preparation of retinal tissue and cells at all developmental stages in the substantial quantities required for clinically useful retinal grafts.

In a study of murine retinal transplantation, Pearson et al. reported that postmitotic photoreceptor precursor cells were able to efficiently integrate into the host retina that retained an outer nuclear layer (ONL) and restore visual function (11). However, the first clinical applications of retinal grafts are likely to be in the treatment of end-stage disease or, more likely, for the replacement of a segment of degenerating retina where photoreceptors or ONLs have been depleted (Fig. S1*A*). The majority of the cases of RP progress slowly over decades with gradual expansion of the degenerative area from the midperipheral areas toward central areas, with many patients having a substantial "ONL-depleted area" surrounding the cone-rich macula for a considerable period before central cone photoreceptors finally degenerate as a secondary change. Assuming that the first clinical applications are likely to be transplantation to the end-stage ONL-depleted host retinas, we recently demonstrated the efficacy of transplantation of murine ESC- or iPSC-derived retinal tissue (mESC/iPSC-retina) in a mouse model of progressive retinal degeneration (*rd1*) or ONL-depleted host

Significance

We first confirmed the ability of human embryonic stem cell-derived retina (hESC-retina) to form structured mature photoreceptor layers after transplantation into nude rats. We then developed two monkey models of retinal degeneration and evaluated their utility as host models for transplantation studies. Finally, we performed a pilot study of hESC-retina transplantation in the developed models and conducted in vivo monitoring studies using clinical devices and subsequently confirmed structured graft maturation and the potential formation of synaptic contacts between graft and host cells. This study demonstrates the competency of hESC-retina as a graft source and the eligibility of two newly developed monkey models that may be useful in future, long-term, functional studies of retinal transplantation.

Author contributions: H.S., M.M., H.T., Y.S., and M.T. designed research; H.S., M.M., K.M., A.K., S.Y., T.N., and J.A. performed research; H.S., M.M., T.K., K.S., M.E., and M.T. analyzed data; and H.S., M.M., and A.K. wrote the paper.

The authors declare no conflict of interest.

This article is a PNAS Direct Submission. D.J.Z. is a guest editor invited by the Editorial Board.

[1]To whom correspondence should be addressed. Email: mmandai@cdb.riken.jp.

This article contains supporting information online at www.pnas.org/lookup/suppl/doi:10.1073/pnas.1512590113/-/DCSupplemental.

retinas. Transplanted mESC/iPSC-retinas developed structured ONL with mature outer segments (OSs) and more or less of inner nuclear layer (INL) components after transplantation. Further, we demonstrated that the structured layers of photoreceptors (ONL) in grafts were in direct, 3D contact with INL of the host retina in cases where graft INLs were stripped off from graft ONLs, an integration process we termed the "direct contact pattern" (14). Detailed observation of the host–graft interface in direct contact pattern indicated the formation of synaptic connections between host bipolar cells and the graft photoreceptors by immunohistochemical analysis. Although this study provided a promising outcome, it remains unclear whether similar results regarding host acceptability and graft competency can be achieved in primate models and human tissue grafts.

In the present study, we demonstrate the ability of hESC-derived retinal sheets (hESC-retina) to survive and fully mature to form structured ONLs with inner segments (ISs) and OSs after transplantation into nude rats. Direct integration of graft photoreceptors with host bipolar cells was observed after transplantation of graft retinas into the subretinal space of an end-stage retinal degeneration immunodeficient rat model [SD-Foxn1 Tg(S334ter)3LavRrrc] (18), indicating the potential utility of hESC-retinas as a graft source.

We further evaluated the utility of hESC-retina transplantation in monkey end-stage retinal degeneration models. Because there are no previously reported monkey models of genetic or spontaneous progressive retinal degeneration, or an adequate injury-inducible retinal degeneration model, we developed two injury-induced focal retinal degeneration models using cynomolgus and rhesus monkeys that allow for detailed monitoring and functional evaluation after retinal transplantation. Focal photoreceptor-selective injury outside the macular region was performed, allowing simulation of retinal tissue transplantation within ONL-depleted perimacular areas, the most likely initial clinical application of retinal grafts. The utility of these currently developed monkey models in retinal transplantation studies was fully evaluated. Further, we simultaneously developed a visual acuity (VA) test that we believe will be of great benefit to future studies. We then conducted a pilot study of hESC-retina transplantation in our monkey models of retinal degeneration. Retinal grafts were monitored in vivo for 1, 3, 4, and 5 mo in four eyes of three monkeys with two types of retinal degeneration models. We subsequently observed the maturation and integration of hESC-retinas in host primate retinas by histological analyses.

Results

Utility of Retinal Sheets Derived from Human ESCs as a Graft Source. Rx::Venus and Crx::Venus ES cell lines (KhES-1) could be reproducibly differentiated into hESC-retinal cells expressing Venus as previously described (Fig. 1 *A* and *A′*) (16). To investigate the maturation and integrative potential of hESC-retinas, we first transplanted hESC-retinas into the subretinal space of

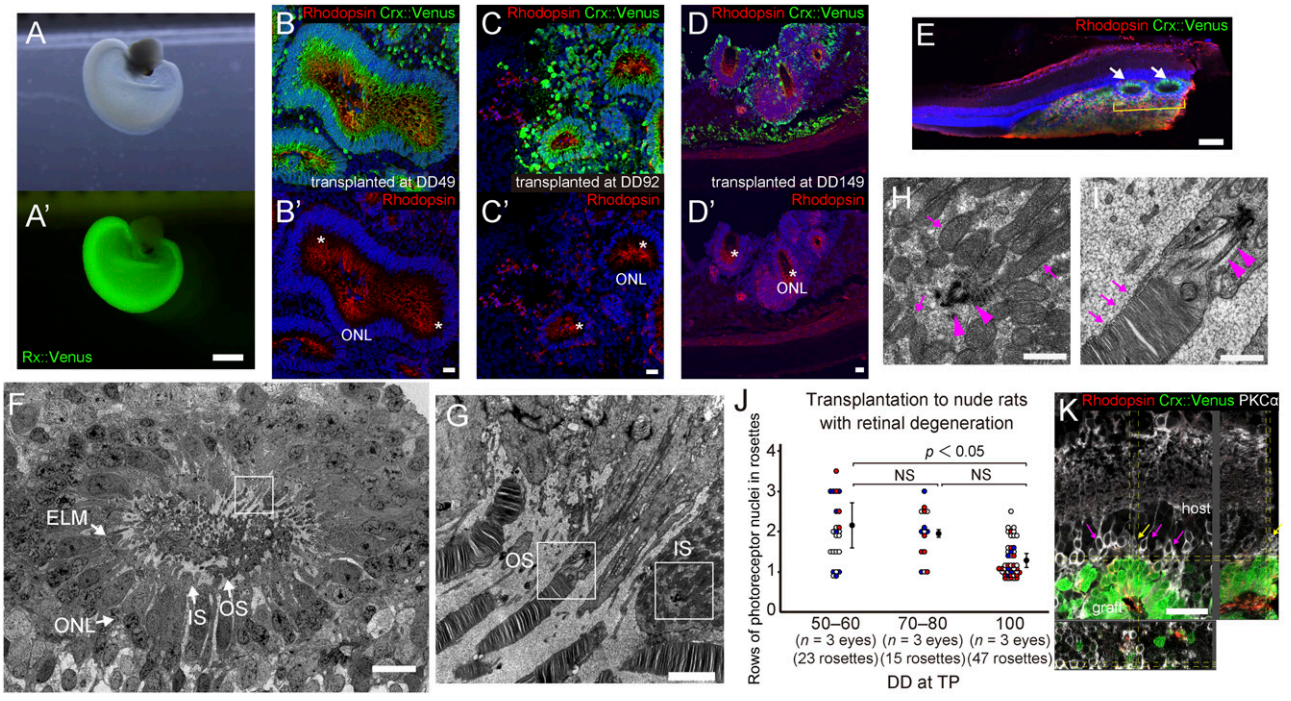

Fig. 1. Maturation of hESC-retinas in the subretinal space of nude rats. (*A* and *A′*) hESC-retina differentiated from Rx::Venus (KhES-1) ES cells. (*B–D′*) The 3D retinal sheets derived from Crx::Venus hESCs were transplanted subretinally at DD49 (*B* and *B′*), DD92 (*C* and *C′*), and DD149 (*D* and *D′*). All grafts expressed rhodopsin in a rosette-like structure at DD215–279. IS/OSs are indicated by asterisks. (*E*) Low-magnification image of transplanted retina with DD293 graft. Typical rhodopsin-positive rosettes were identified (arrows) and processed for electron microscopy. The retinal sheet was transplanted at DD105. (*F*) Magnified view of the rhodopsin-positive rosette with electron microscopy. The graft was observed to form ONL structure with external limiting membrane (ELM), IS, and OS. (*G*) High-magnification image of IS–OS connections shown in the boxed region of *F*. (*H and I*) High-magnification images of the boxed regions in *G*. IS contained mitochondria (*H*, arrows), and OS consisted of typical stacks of discs with continuous plasma membrane (*I*, arrows) from connecting cilia (*H* and *I*, arrowheads). (*J*) hESC-retinas were transplanted into SD-Foxn1 Tg(S334ter)3LavRrrc rats, an immunodeficient end-stage retinal degeneration model. ONL thickness indicated as number of rows of nuclei was counted in all rosettes in a 50-μm section per eye at DD240–270 after transplantation of grafts at the indicated DD. Individual data points are plotted (rosettes from the same eye are indicated by the same color). The numbers of rows were averaged per each eye, and mean ± SD of the eyes in each group was presented. Statistical significance was accessed by ANOVA with Student–Newman–Keuls test. (*K*) The graft ONL presented a typical direct integration with host bipolar cells (yellow and purple arrows) at DD241 after transplantation of grafts at DD102 into nude rats with retinal degeneration. Nuclei were stained with DAPI (blue). [Scale bars: 500 μm (*A*), 20 μm (*B–D′*), 100 μm (*E*), 10 μm (*F*), 2 μm (*G*), 0.5 μm (*H* and *I*), and 20 μm (*K*).]

nude rats. Initially, transplanted grafts of differentiation day (DD) 60–120 at the time of transplantation (TP) were studied; however, confirmative expression of rhodopsin was not detected at approximately DD90–100 (DD60 at TP; $n = 4$), or DD140–150 (DD88 at TP; $n = 2$, and DD110–120 at TP; $n = 6$, respectively). Because weak rhodopsin expression has been reported at approximately DD130 in vitro (15, 16), we next transplanted grafts of DD140 into nude rats and performed histological analyses at DD200–210 ($n = 6$). These analyses demonstrated partial, but evident, expression of rhodopsin and the presence of OS-like structures within most rosettes, indicating that a substantial period is required for the maturation of hESC-retinas. We next evaluated grafts of approximately DD50 ($n = 2$ Crx::Venus ESC-retina), DD100 ($n = 4$ Crx::Venus ESC-retina, $n = 1$ Rx::Venus ESC-retina), and DD130–150 ($n = 2$ Crx::Venus ESC-retina, $n = 3$ Rx::Venus ESC-retina), with histological analyses performed at DD215–279. All grafts developed rhodopsin-positive ONL in almost all rosette-like structures. IS/OS-like structures were also observed in the majority of rosette-like structures (Fig. 1 *B–D′*, asterisks). Electron microscopy of a rosette (Fig. 1 *E* and *F*) confirmed the development of IS and OS connected by cilia (Fig. 1*G*). IS was found to contain mitochondria (Fig. 1*H*, arrows), whereas OS was composed of well-aligned membranous discs (Fig. 1*I*, arrows), indicating terminal photoreceptor maturation. The grafts of approximately DD50 at TP were observed to develop thick ONLs of four to six rows that were not seen in the grafts of DD100 or DD150 at TP (Fig. 1*B* and Fig. S1*B*). Also, the proportion of cones in rosettes was ∼10% in the grafts of DD50 at TP (Fig. S1*C*). Considering that the clinical application where shorter culture period may be preferred, graft DD at TP was fixed up to approximately DD100 hereafter. Our previous study of mESC/iPSC-retina demonstrated that structured graft ONL was either prevented from reaching the host INL by the presence of graft INL components (laminar interception pattern) or able to contact the host INL with graft INL "peeled off" from the graft ONL (direct contact pattern) (14). We evaluated the presence of similar patterns after the transplantation of hESC-retinas of DD50–60, DD70–80, or approximately DD100 in nude rats with a rho mutation, SD-Foxn1 Tg(S334ter)3LavRrrc, as a model of end-stage retinal degeneration. With degenerating thin retina in the mutant host rats, we could directly observe rosettes of different sizes formed in graft sheets under the stereo microscope (Fig. S1*D*). Grafts of DD50–60 at TP developed thicker ONLs than those of DD100 at TP that had greater number of small rosettes (ANOVA, $P < 0.05$; Fig. 1*J*), and rosettes with thick ONL often had rows of INLs (Fig. S1 *E–F′*, arrows). With hESC-retinas, the peeled-off phenomenon was not evident, and it was often difficult to clearly distinguish the direct contact pattern from the laminar interception pattern, with different degrees of graft inner cells consistently remaining and residing in proximity with host inner cells. Nonetheless, contact between host bipolar dendrites and graft ONL or photoreceptor cells, which we termed direct integration, was observed in a proportion of rosettes (Fig. 1*K*, arrows). When the ratio of rosettes with direct integration among all of the rosettes adjacent to host retina was estimated from a number of representative sections (average of 11 rosettes per eye were evaluated), grafts of DD50–60 at TP were found to have a comparable ratio of direct integration with other DDs at TP (Fig. S1*G*). Based on these background data, we decided to use hESC-retinas of approximately DD50–60 in subsequent monkey transplantation studies.

Cobalt Chloride-Induced Retinal Degeneration Model. To test retinal grafts in monkeys, we developed two retinal degeneration models. Intravitreal injection of cobalt chloride has been reported to induce photoreceptor degeneration in rodents (19). Because we were unable to induce full-thickness ONL degeneration with intravitreal injection of cobalt chloride in monkeys, we attempted to create a retinal degeneration model using subretinal injection of cobalt chloride. Although administration of 40 μL of 0.40 mg/mL cobalt solution resulted in both ONL and INL degenerations, 0.20 mg/mL cobalt solution did not result in ONL eradication (Fig. S2*A*). Therefore, further studies were performed by using either 0.25 or 0.30 mg/mL cobalt solution. After treatment with either concentration, discolored lesions immediately developed that then became less evident between 2 and 7 mo after intervention (Fig. 2*A*), without evidence of leakage or blockage on fluorescein angiography (FA) (Fig. 2*B*). Radial optical coherence tomography (OCT) demonstrated uniform, central loss of ONL at injury sites (Fig. 2*C* and Fig. S2*B*, black circles), surrounded by circular areas that were partially affected with variable loss of ONL (Fig. 2*C* and Fig. S2*B*, green circles; Fig. S2*C*). ONL thickness decreased during the first week after injury, but remained stable for up to 7 mo thereafter. INL appeared normal throughout the observation period. (Fig. 2*C* and Fig. S2 *B* and *C*). Focal cone electroretinograms (ERGs) of lesions were recorded with 15° spot stimulation, smaller than the areas of ONL degeneration. Positive controls were recorded at identical regions in normal monkeys. At all times after injury with either concentration of cobalt solution, the a-and b-waves were nonrecordable; however, a slight photopic negative response was detected at 3 and 7 mo after treatment with 0.25 mg/mL cobalt solution (Fig. 2*D*). At 3 mo after injection of 0.30 mg/mL cobalt solution, histological analysis revealed almost complete ONL loss in central lesions with increased glial fibrillary acidic protein (GFAP) expression (Fig. S2 *D* and *E*); however, the expression of other retinal cell markers of the inner layer, including calretinin, calbindin, protein kinase C (PKC)-α, and recoverin, was maintained, indicating the presence of amacrine, horizontal, and rod and cone bipolar cells, respectively. Retraction of PKC-α–positive bipolar cell dendrites was observed (Fig. 2*K* and Fig. S2 *F* and *H*). Microglial accumulation, determined by ionized calcium-binding adapter molecule 1 (Iba1) expression, was not observed (Fig. 2*K*). RPE65-positive cells were present at injury sites (Fig. S2*G*). At 7 mo, calretinin expression was negative with injection of 0.30 mg/mL cobalt solution (Fig. 2*H* and Fig. S2*F*). No PKC-α expression was observed after injection of either 0.25 or 0.30 mg/mL cobalt solution (Fig. S2*I*), in addition to ONL loss and increased GFAP expression (Fig. 2 *E–G* and Fig. S2 *D* and *E*), indicating secondary loss of amacrine and bipolar cells. Calbindin and recoverin expression in the inner layer at this time point indicated the presence of horizontal and cone bipolar cells, respectively (Fig. 2*J* and Fig. S2*H*). RPE65-positive cells were present at injury sites (Fig. 2*I* and Fig. S2*G*), with minimal activation of microglia observed by Iba1 immunohistochemistry (Fig. S2*I*). Cobalt chloride-induced ONL degeneration was confirmed in three other eyes, with quantitative temporal changes in ONL thickness consistent across all eyes (ANOVA, $P < 0.01$; Fig. S2 *J* and *K*). Negative focal ERG corresponding to each injury site was also confirmed in these eyes.

A 577-nm Optically Pumped Semiconductor Laser-Induced Retinal Degeneration Model. Focal photoreceptor degeneration was observed after photocoagulation with a 577-nm optically pumped semiconductor laser (OPSL). Fundus imaging demonstrated focal white-colored lesions at 4 d after intervention that became progressively less evident over the subsequent 2 mo. Autofluorescence imaging demonstrated hyperfluorescence at injury sites at 4 d after intervention that became hypofluorescent over the subsequent 2 mo (Fig. 3*A*). FA revealed no evidence of active injury, such as choroidal neovascularization, during the 2 mo after injury (Fig. 3*B*). Chronological observation with OCT demonstrated enhanced OCT signals in ONL at 4 d, followed by rapid ONL loss over the subsequent 2 wk, whereas the inner layer appeared well preserved. ONL under vessels appeared

to be less affected (Fig. 3*C*, arrowheads). Uniform degeneration, confirmed by radial OCT imaging, was observed over the affected area (Fig. S3*A*). By using focal cone ERGs, 15° spot stimuli well within lesions were found to evoke the slight a- and b-wave at 2 wk after injury; however, responses became almost nonrecordable thereafter throughout the experimental period (Fig. 3*D*). Immunohistochemical analyses revealed that lesions at 76 and 138 d have similar retinal cell

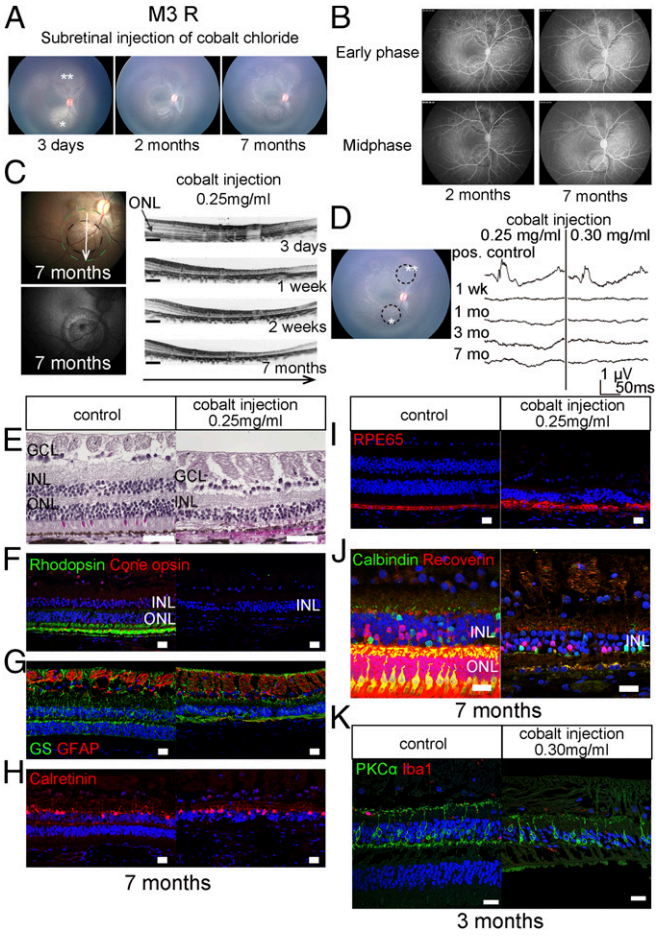

Fig. 2. Retinal degeneration induced by subretinal injection of 0.25 and 0.30 mg/mL cobalt chloride solution. (*A*) Fundus photographs of lesions induced by subretinal injection of cobalt solutions at 3 d, 2 mo, and 7 mo after intervention. (*B*) FA images at ∼30 s (early phase) and 2 min (midphase) after injection of sodium fluorescein at 2 and 7 mo after injection of cobalt solution demonstrated no leakage. (*C*) Time course of OCT imaging of a lesion induced by 0.25 mg/mL cobalt solution indicated by the arrow on the fundus photograph is shown in *Right*. High signals were observed in the ONL at 3 d after intervention. The ONL was completely lost at 1 wk and stabilized thereafter. (*Left Upper*) Fundus photograph at 7 mo demonstrating an area of almost complete ONL loss but sparing of the inner cell layer surrounding a lesion (black circle) and moderately affected marginal area (green circle). (*Left Lower*) Autofluorescent imaging demonstrating sparse lesional hyperfluorescence and hypofluorescence. (*D*) Focal ERGs were recorded with a 15° spot stimuli (black circle on the fundus photograph) after subretinal injection of cobalt solution. The a- and b-waves were almost nonrecordable at all times after injury. (*E*–*K*) Histological images of injury sites induced by cobalt chloride compared with intact areas of the same retina. (*E*) Injection of cobalt solution leads to ONL-selective degeneration as demonstrated by hematoxylin and eosin (H&E) staining of retinal sections. (*F*–*J*) Retinal sections were stained for rhodopsin and cone opsin (*F*), GS and GFAP (*G*), calretinin (*H*), RPE65 (*I*), and calbindin and recoverin (*J*) 7 mo after injection of 0.25 mg/mL cobalt solution. (*K*) Retinal sections were stained with PKC-α and Iba1 3 mo after injection of 0.30 mg/mL cobalt solution. Nuclei were stained with DAPI (blue). [Scale bars: 500 μm (*C*), 50 μm (*E*), and 20 μm (*F*–*K*).]

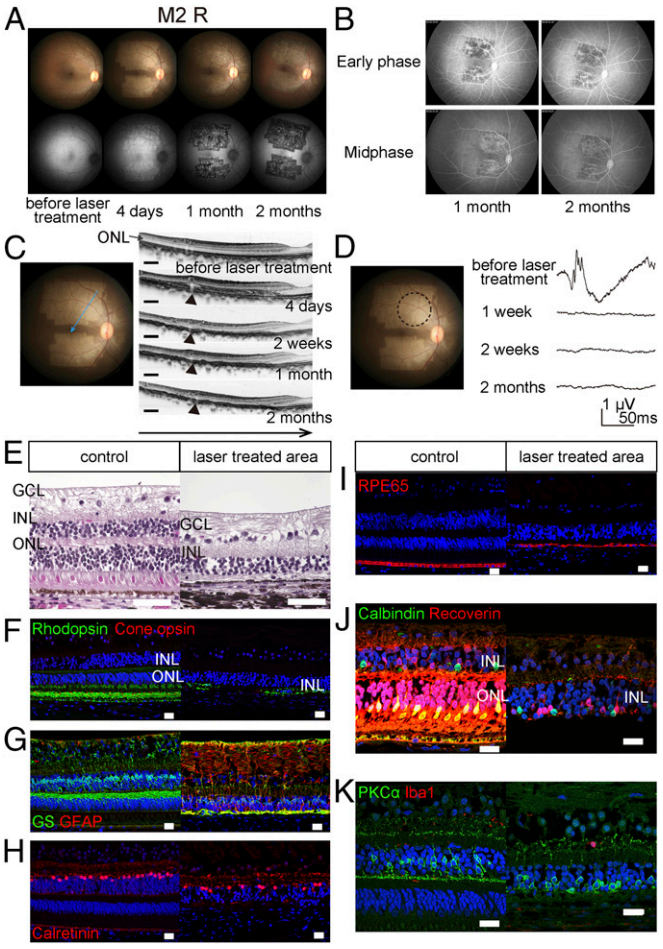

Fig. 3. Laser photocoagulation selectively induces local photoreceptor degeneration. (*A*) Representative fundus photographs (*Upper*) and autofluorescence images (*Lower*) before and at 4 d, 1 mo, and 2 mo after intervention. (*B*) FA imaging of the laser-injured retina at 1 and 2 mo revealed no hyperfluorescence. (*C*) Sectional views of OCT imaging of the locus indicated by the arrow on the fundus photograph before and at 4 d, 2 wk, 1 mo, and 2 mo after injury. The ONL thickness had dramatically declined by 2 wk. ONL immediately deep to large vessels was less affected (arrowheads). (*D*) Focal ERGs of degenerative area with a 15° spot stimuli (circle on the fundus photograph) before and at 1 wk, 2 wk, and 2 mo after laser treatment. Focal ERGs were almost nonrecordable at all times after injury ($n = 4$ eyes). (*E*–*K*) Histological images of retinas from the laser model compared with positive controls. (*E*) Representative images of H&E-stained retinal sections, showing ONL-selective injury. (*F*–*K*) Retinal sections were stained with rhodopsin and cone opsin (*F*), GS and GFAP (*G*), calretinin (*H*), RPE65 (*I*), calbindin and recoverin (*J*), and PKC-α and Iba1 (*K*). Nuclei were stained with DAPI (blue). [Scale bars: 500 μm (*C*), 50 μm (*E*), and 20 μm (*F*–*K*).]

marker expression profiles. Laser treatment was found to selectively reduce ONL thickness with preservation of the ganglion cell layer (GCL) and INL (Fig. 3*E*); however, the degree of degeneration was not homogeneous, with focal regions of photoreceptor sparing demonstrated by the expression of opsin markers (Fig. 3*F* and Fig. S3*B*). Uneven damage to RPE65-positive cells was also detected (Fig. 3*I* and Fig. S3*C*). GFAP expression was enhanced in Muller cells (Fig. 3*G*). Other retinal markers, including calretinin (amarcrine cells), calbindin (horizontal cells), recoverin (off cone bipolar cells), and PKC-α (rod and cone bipolar cells), were all expressed in injured areas, although retraction of PKC-α–positive bipolar cell dendrites was observed (Fig. 3 *H*, *J*, and *K*). Minimal increases in the number of Iba1-positive microglia were observed (Fig. 3*K*). Consistent temporal changes in ONL thickness measured by OCT images

(ANOVA, $P < 0.01$; Fig. S3 *D* and *E*) and negative focal ERGs were confirmed in three additional laser-treated eyes.

Maintenance of VA in Retinal Degenerational Model. Because focal ONL degeneration is induced outside the fovea, demonstration of the preservation of central vision would ensure the safety of the present study and allow essential perimetric analyses in future studies (20). Thus, we developed a protocol to evaluate the VA of monkey eyes based on human VA tests. A special cage was made to independently evaluate VA in each eye with a maximum VA detection capability of logMAR 0.7 (Fig. S4 *A–E*). Monkeys were trained to distinguish a Landolt circle from complete circles before intervention (Movie S1). After laser and cobalt treatment, VA was tested in each eye (Movies S2 and S3). Although decreases in VA were observed immediately after the intervention, foveae remained unchanged, as confirmed by OCT (Fig. S4*F*), and VA returned to normal by 3 wk after injury in all models (Table S1).

Transplantation of hESC-Retinas into Developed Monkey Models. We then performed a pilot study of hESC-retina transplantation in one eye of the laser-induced model and three eyes of the cobalt-induced retinal degeneration models in monkeys (M1–M3; Table S2). Degenerative sensory retinas could be safely detached from the RPE in both models before the placement of Rx::Venus+ or Crx::Venus+ hESC-retinas at approximately DD60 into the subretinal space (Movie S4). OCT imaging demonstrated the presence of graft retina-like sheets in regions where the host ONL was substantially degenerated (Fig. 4 *A, B, D,* and *E* and Fig. S5*A*). Cyclosporine, an immunosuppressant, was administered in both models, with monitoring of serum levels to maintain levels >80–100 ng/mL. FA revealed no evidence of rejection in any of the transplanted eyes (Fig. 4 *C* and *F* and Fig. S5*B*). The thickness of grafts consistently increased until approximately DD120 and remained stable thereafter (Fig. 4 *G* and *H*). Focal ERG did not yield positive results in the present pilot study. Monkeys were euthanized, and eyes were harvested at 35, 88, 123, and 148 d after transplantation (graft ages of DD90, DD148, DD182, and DD210, respectively) for immunohistological analysis. Although proliferating (Ki67-positive) cells were predominantly present within rosettes at DD90, the number of proliferating cells was significantly lower in DD148 sample, and no Ki67-positive cells were observed in rosettes at DD182 and DD210 (Fig. 5*A*), consistent with the temporal change in the thickness of transplanted grafts observed on OCT (Fig. 4*G*). Only a few Ki67-positive cells were observed outside rosettes in any grafts. In the laser model, rosettes in the graft of DD90 were all positive for recoverin (Fig. 5*B*); however, no expression of rhodopsin or cone opsins was observed, indicating that photoreceptor cells remained immature at this time point. Nevertheless, dendrites of bipolar cells were observed extending into ONL (arrows) to form direct contact with graft Rx::Venus+ cells (Fig. 5*C*). In the cobalt model, each of the DD148, 182, and 210 grafts was found to express Rx::Venus or Crx::Venus and recoverin in all rosettes and ONL-like structures. Rosettes in grafts expressed mature photoreceptor markers, such as rhodopsin, s-opsin and m/l-opsin, with the development of IS/OS-like structures (Fig. 5 *D–G*, asterisks). Mutually exclusive expression of rod and cone markers was observed by immunohistochemistry (Fig. S5*C*). At DD148, 182, and 210, possibly developing IS/OS structures of rod photoreceptors were also stained with peripherin-2 and transducin (Fig. 5 *H–H′* and Fig. S5 *D–F′*). The proportions of rosettes positive for recoverin, rhodopsin, and cone opsins in each sample are summarized in Fig. 5*I*, with all rosettes positive for both rod and cone markers at DD210 (Fig. S5*G*). The mean proportions of cones in rosettes were 9.4 ± 3.0%, 12.2 ± 2.4%, and 15.2 ± 5.6% at DD148, DD182, and DD210, respectively (mean ± SD; Fig. 5*J*). Grafts were also observed to express inner cell markers, including

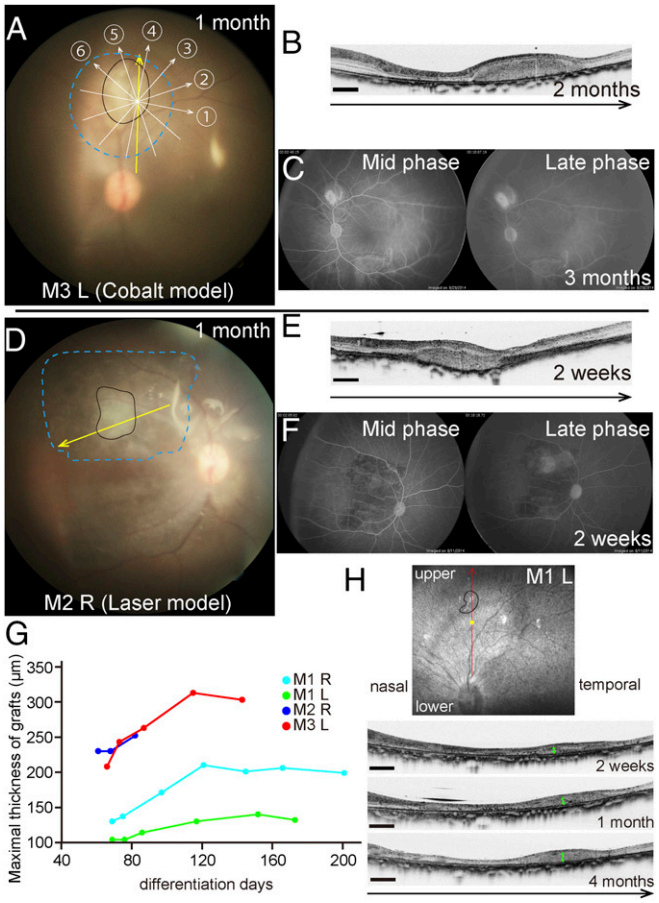

Fig. 4. In vivo imaging of hESC-retinas after transplantation. (*A–C*) Representative fundus photograph (*A*), OCT image (*B*), and FA images (*C*) of the transplanted graft in the monkey cobalt model (M3L). All OCT radial images are shown in Fig. S5*A*. (*D–F*) Fundus photograph (*D*), OCT image (*E*), and FA images (*F*) of the transplanted graft in the laser model (M2R). The grafts (black outlines; *A* and *D*) were located in the subretinal space of degenerative retinas (blue outlines; *A and D*). (*G and H*) The maximal thickness of grafts was evaluated by OCT in the same section view of each eye after transplantation. (*G*) Line graph of temporal changes in graft thickness for each transplanted eye. (*H*) Representative OCT images showing graft thickness in M1L. [Scale bars: 500 μm (*B*, *E*, and *H*).]

calretinin, calbindin, and PKC-α, indicating intragraft structured maturation (Fig. 5 *K–M*). Intragraft synaptic connections between graft photoreceptors and graft bipolar cells were also detected by immunohistochemical staining for PKC-α and RIBEYE, a component of synaptic ribbons with a characteristic horseshoe pattern of staining at photoreceptor terminals (21), indicating that graft photoreceptors were sufficiently mature to form synaptic connections (Fig. 5*M*). Some of graft cells expressed glutamine synthetase (GS) and GFAP; however, we were unable to determine whether these cells were derived from host or graft cells. In either case, GS- and GFAP-positive host Muller glia did not appear to block the integration of, or invade into, rosette-like structures of the graft tissue (Fig. 5*N*). The number of host PKC-α–positive cells was decreased in the cobalt model; however, intimate interactions between host and graft cells were detected in regions where host bipolar cells were preserved. Photoreceptor cells, coexpressing human markers and recoverin, were found to be in contact with host bipolar dendrites (Fig. 6 *A* and *B*) adjacent to rhodopsin-positive rosettes (Fig. 6*C*). Host bipolar cells were observed extending dendrites to graft cells and to ONL (Fig. 6*C*, arrows). Ribbon synapses,

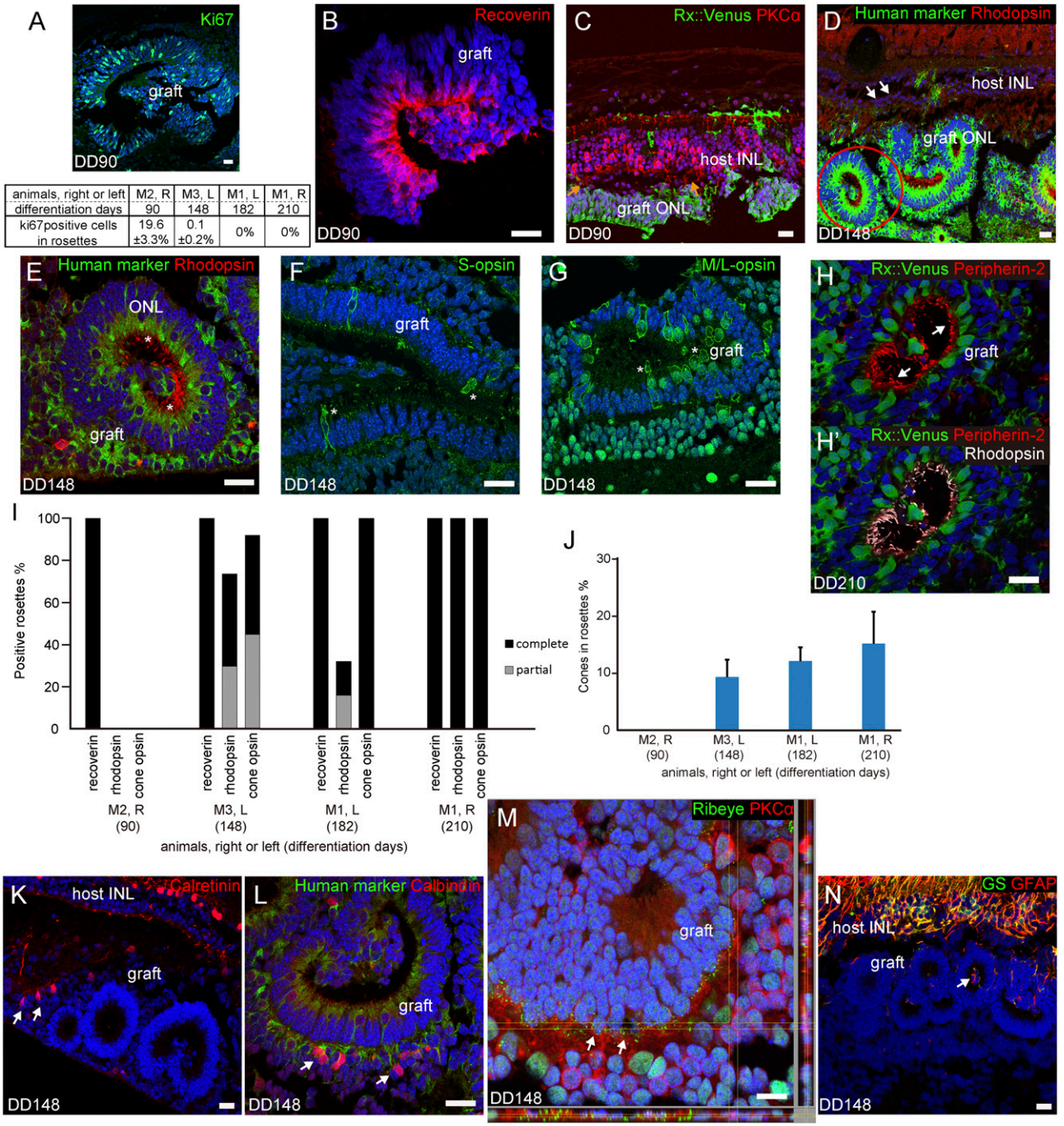

animals, right or left	M2, R	M3, L	M1, L	M1, R
differentiation days	90	148	182	210
ki67positive cells in rosettes	19.6 ±3.3%	0.1 ±0.2%	0%	0%

Fig. 5. Maturation of transplanted hESC-retinal sheets in degenerative monkey retinas. (*A*) Representative image of Ki67$^+$ cells in a rosette at DD90. Proportion of Ki67$^+$ cells in rosettes from grafts at differing DD (mean ± SD, $n = 9$). (*B*) Graft at DD90 in the laser model (M2R) expressed recoverin. (*C*) Host bipolar cell dendrites observed extending into the graft ONL (arrows) at DD90. (*D*) Rx::Venus hESC-retina observed to survive in the subretinal space of a degenerative monkey retina in the cobalt model observed to express the human marker (SC121) and rhodopsin at DD148 (M3L). Graft ONL was observed adjacent to host INL (arrows). High-magnification image of the rosette demarcated by the red circle is shown in *E*. (*E*–*G*) Structured ONL in rosette-like forms derived from a transplanted graft expressed rhodopsin (*E*), s-opsin (*F*), and m/l-opsin (*G*) at DD148. IS/OSs are indicated by asterisks. (*H* and *H'*) IS/OS formation was suggested by peripherin-2 expression observed at DD210 (M1R). (*I*) Proportion of rosettes positive for each photoreceptor marker (recoverin, rhodopsin, and cone opsin) at each graft DD. The positivity of rosettes was categorized as either complete (evenly expressed throughout a rosette) or partial. (*J*) Proportion of all DAPI$^+$ cells positive for either s-opsin or m/l-opsin in each positive rosette (mean ± SD, $n = 9$). (*K* and *L*) Amacrine and horizontal cells observed within the graft at DD148, as demonstrated by calretinin (*K*) and calbindin (*L*) immunohistochemistry. (*M*) Intragraft synaptic formation demonstrated by colocalization of the presynaptic marker, Ribeye, and the bipolar cell marker, PKC-α at DD148. (*N*) Weak expression of GS and GFAP observed in rosette-like structures at DD148. Nuclei were stained with DAPI (blue). [Scale bars: 20 μm (*A*–*H'*, *K*, *L*, and *N*) and 10 μm (*M*).]

indicated by RIBEYE expression, were also observed at sites of interaction between host bipolar dendrites and graft Rx::Venus-positive cell axon terminals (Fig. 6 *D*–*D″*). Possible direct integration of graft photoreceptors with host bipolar cells was observed in a number of graft locations where graft INL components, including graft bipolar cells, did not evidently block

contact between host bipolar cells and graft ONL (Fig. 5*D* and Fig. 6*E*, arrows).

Discussion

As a preparative study assessing the clinical utility of hESC- and hiPSC-derived retinal transplantation, we first confirmed the competency of hESC-retinas as a graft source in nude rats. We then developed and evaluated the utility of two monkey models of retinal degeneration for use in transplantation studies. We next performed a pilot study of hESC-retina transplantation and demonstrated that grafts could survive, mature, and possibly integrate with host bipolar cells in eyes of the developed monkey models.

The lack of adequate monkey retinal degeneration models has been a substantial drawback of retinal transplantation studies regarding the assessment of the potential clinical feasibility of this therapeutic strategy. The retinas of rodents and primates substantially differ, including in the distribution of rods and cones, and the induction of selective, yet complete, photoreceptor degeneration is technically challenging in primates. Several monkey retinal degeneration models have been reported, including systemic injection of iodoacetic acid (IAA) (22), light-induced retinal damage using intraocular fiber optics (23), and focal damage by severe light exposure (24). However, these models had one or more features of being unethical, unstable, irreproducible, or unable to produce adequately sized lesions. The requirements for a monkey retinal degeneration model for use in transplantation studies should include the following aspects: photoreceptors should degenerate selectively and consistently while preserving secondary and other neuronal cells; the model should enable us to mimic clinical surgical procedures allowing outcome and safety studies; the model should allow the detection of focal recovery of light responsiveness, ideally allowing clinically relevant functional studies; and visual impairment should be focal or in a single eye for ethical reasons.

In the present study, we developed RP models using two approaches: subretinal injection of cobalt chloride, a hypoxia-mimicking agent that induces HIF-1α (25), and 577-nm OPSL photocoagulation. Subretinal injection of a hypoxia-mimicking agent represents a proposed method of selectively damaging ONL that is supported by choroidal circulation when oxygen is supplied to the GCL and INL by retinal vessels (26). We also attempted to damage photoreceptors using blue light and intraocular fiber-optic light; however, the degree of photoreceptor damage was minimal. Cobalt and laser models fulfilled the requirements listed above and consistently resulted in sufficiently

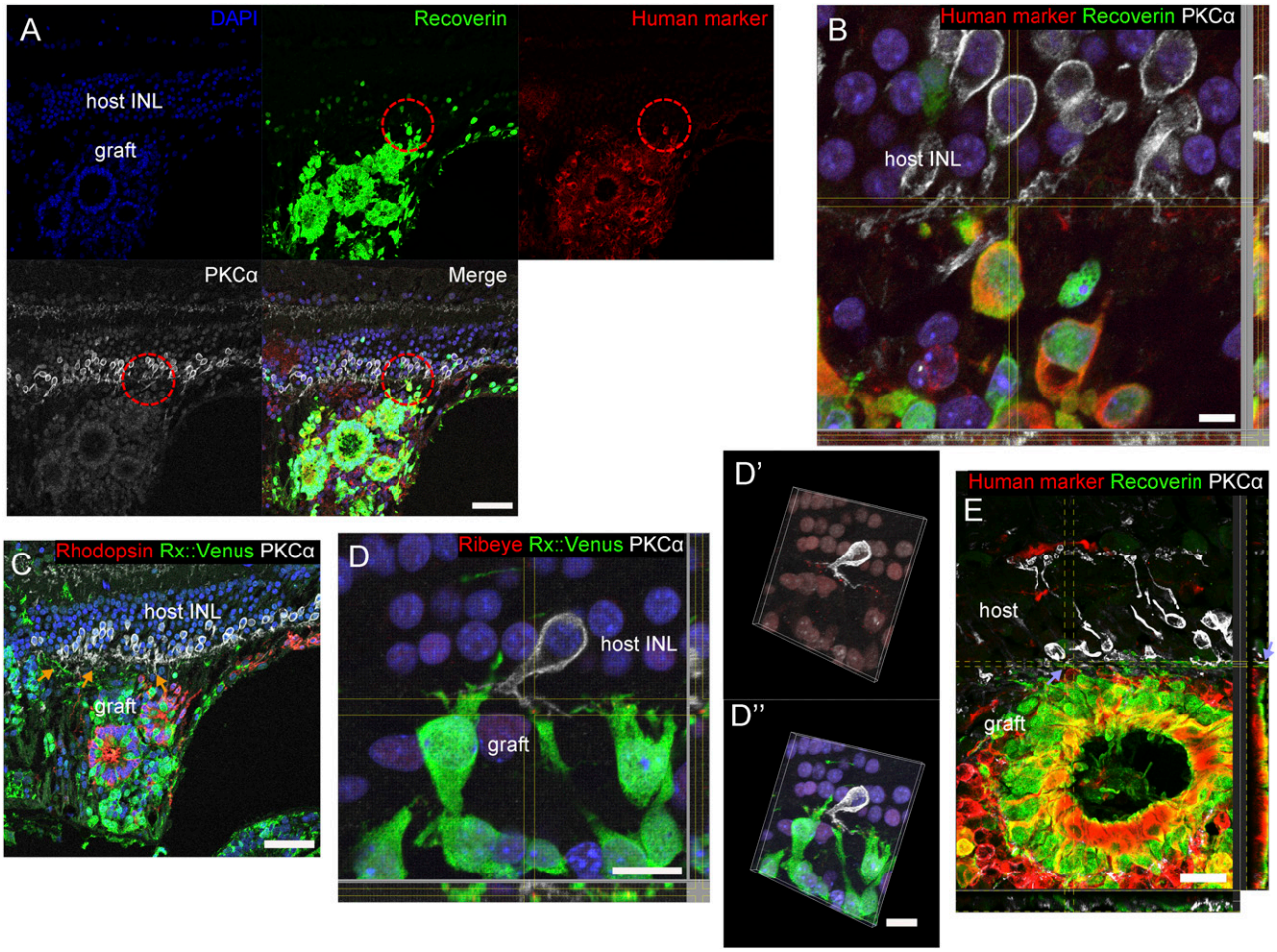

Fig. 6. Contact between host bipolar cells and recoverin-positive graft photoreceptors. (*A*) Cells expressing human markers observed in contact with host PKC-α–positive bipolar cells at DD148 (M3L). (*B*) High-magnification image of the circled area in *A*. Interactions observed between recoverin-positive graft cells and host bipolar cells. (*C*) Graft expressing rhodopsin with sprouting of host bipolar cells into graft areas (arrows) at DD148. (*D*–*D*″) Host PKC-α–positive cell in contact with graft Rx::Venus-positive cells with localization of the presynaptic marker, Ribeye, to dendrite tips of host bipolar cells indicating the formation of synaptic connections between host and graft cells at DD148. (*E*) Representative image of possible direct integration between host INL and graft rosettes at DD210 (M1R). Nuclei were stained with DAPI (blue). [Scale bars: 50 μm (*A* and *C*), 5 μm (*B*), 10 μm (*D*–*D*″), and 20 μm (*E*).]

large areas of photoreceptor-selective degeneration for graft tissue to be placed inside the degenerative areas. Retinas could safely be detached from the RPE without undesirable adhesion during the transplantation procedure in both models. Importantly, because rod-rich graft tissues would be transplanted into the perimacular region in patients with RP in initial clinical trials, we induced focal degeneration in these areas while sparing central vision. The induction of focal perimacular degeneration is not only ethically preferable, but also allows detailed analyses, such as perimetric analysis, which may detect the loss or recovery of focal retinal function (20). The VA test we developed may have utility in future studies evaluating cone function in other models of retinal degeneration involving the central area. Although we had observed a transient decrease in VA in one eye after injury, probably due to mild inflammation, no changes in foveal OCT were observed (Fig. S4*F*), and VA fully recovered in 3 wk.

The models developed in the present study have a few limitations. In the cobalt model, the cobalt chloride effective dose window was found to be extremely narrow. Almost complete loss of photoreceptors in the cobalt model was apparently associated with damage to the inner layer (Fig. 2 and Fig. S2). Conversely, in the laser model, the inner layer was almost entirely preserved; however, photoreceptor loss was occasionally insufficient (Fig. 3 and Fig. S3). These contrasting results may indicate coexistence of complete photoreceptor depletion, and adequate preservation of secondary neurons may be difficult to achieve in these injury models without the use of genetic engineering.

The greatest advantage of hESC-retina lies in the ability to obtain grafts of any developmental stage in any desirable form in practical quantities by using 3D differentiation culture. Transplantation of human fetal retinas has been performed with a degree of efficacy in some countries (27–29); however, in addition to ethical issues, the detailed mechanisms underlying the contribution of graft tissue to reported outcomes were not conclusive, partly due to a lack of tools of detailed analysis at the time. Thus, survival, maturation, and integration competency of hESC-retina after transplantation should be further studied in primate models to identify potential clinical applications. We transplanted hESC-retinas into nude rats to determine the most efficacious DD stage for transplantation and found that retinal tissue of any development stage between DD50 and DD150 was able to fully mature and form IS/OS structures in rosettes at DD215–279, with a tendency for younger grafts at TP to develop thicker ONL and substantial numbers of cones (Fig. S1 *B* and *C*). We previously reported that mESC/iPSC-retinas of younger DD at TP were more likely to develop full INL (14). Similarly, younger hESC-retina apparently developed thicker inner cells that may consequently support healthy thick ONL (Fig. S1 *E–F′*). Although inner cells may block host INL–graft ONL contact, rosettes in hESC-retina of DD50–60 at TP had a comparable percentage of direct integration with host bipolar cells to those of older DDs at TP (Fig. S1*G*). Based on these data, we decided to transplant hESC-retinas into the developed monkey models at approximately DD60. Our experience of mESC/iPSC-derived retina indicates that hESC-retinas are likely capable of developing fully organized OS if properly settled on the RPE (14). ONLs from grafts of DD50–60 at TP seemed less thick when transplanted in degenerating retina than those transplanted in wild-type retina (Fig. 1*J* and Fig. S1*B*). The possible decrease in ONL thickness could be due to the degenerating host environment or could be related to the loss of support of intragraft inner cells when graft ONLs were in the process of rewiring to host inner cells.

Because grafts of DD60 are immature, we evaluated undesirable proliferation after transplantation into primate models. Both in vivo observation by OCT and temporal changes in the proportion of Ki67-positive cells (Fig. 4*G* and Fig. 5*A*) indicated that graft cell proliferation was developmental, with no tumor formation observed. With immunohistochemistry, all rosettes became positive for cone opsin at DD182 and for both rod and cone opsin at DD210 (Fig. 5*I*). This result indicates that cones in the graft may mature earlier than rods. Even at DD148, considerable numbers of rosettes were positive for rhodopsin, suggesting that photoreceptors may mature faster in immune-suppressed monkeys than in nude rats, in which we observed the presence of rhodopsin-positive rosettes only after DD200. Rod photoreceptors were also positive for peripherin-2 and transducin at DD148, 182, and 210 (Fig. 5 *H* and *H′* and Fig. S5 *D–F′*). Given the OS structures observed by electron microscopy in the rat study (Fig. 1 *F, G,* and *I*), this staining is suggestive for the presence of mature OS structures in primate transplants. Additionally, activated Muller cells expressing GFAP were not observed blocking, invading into, or encapsulating graft rosette-like structures (Fig. 5*N*). The immune-competent nature of structured retinal tissue may also contribute to long-term cell survival (30), thereby providing sufficient time for hESC-retina to develop mature photoreceptors. The presence of cone photoreceptors in graft tissues, as demonstrated by both s- and m/l-opsin, indicates the potential feasibility of cone function restoration in addition to the restoration of rod function.

Grafts were also positive for RIBEYE and PKC-α (Fig. 5*M*) at DD148, which was not observed during in vitro 3D culture (15, 16). We believe the expression of these factors is essential for host–graft synaptogenesis because, in our previous study using mESC/iPSC-retina, intragraft synapses were always present adjacent to possible host–graft synapses associated with "stripped off" graft INLs, indicating that either "synaptic switching" or host–graft competitive synaptic displacement may take place in the process of host–graft synapse formation around the time of intragraft developmental synaptogenesis (14). Conversely, on the host side, the sprouting of once-retracted host bipolar cell dendrites into graft rosettes was an interesting finding of the present study (Fig. 5*C* and Fig. 6 *A–C*). The retraction of host bipolar cell dendrites has been reported in degenerative conditions, such as in the *rd* mouse and P23H rat models (31, 32). Similar retractions were also observed in both of our developed monkey models (Fig. 2*K* and Fig. 3*K*). Bipolar dendrite sprouting has been reported in normal aged mice and humans (33, 34), occasionally with synaptic remodeling and the formation of ectopic synapses (35), indicating the ability of host bipolar cells to integrate with graft photoreceptors. Indeed, the "rewiring" of bipolar cells to photoreceptors has been suggested in studies of photocoagulated rabbit retinas (36, 37). Dendrite sprouting by host bipolar cells was also observed in our previous study of mESC/iPSC-retina transplantation in *rd1* mice, with the presence of synaptic connections confirmed by immunohistological analysis (14). These findings imply that host bipolar cells with sprouting dendrites may be able to form synapses with graft photoreceptors if sufficiently differentiated into appropriate stages for synaptogenesis and in the correct location.

Although we observed the possible integration of graft photoreceptors with host bipolar cells in a substantial proportion of the grafts in monkey models (Fig. 6 *A–E*), we were unable to determine the frequency of this event due to the limited number of samples; we could not prepare thick 50-μm sections that we routinely use to evaluate host–graft integration using 3D immunohistological analysis by tracing the host bipolar cells traveling through host retina to dendrite tips that contact with graft photoreceptors in eyes of mice (14) or in nude rats with retinal degeneration (Fig. 1*K*). Nevertheless, functional integration of a graft should be further evaluated by a further extensive series of studies, including histological evaluations of the frequency of synapse formation, electrophysiological studies including focal ERGs, and subjective tests such as microperimetry test. In the present study, failure to detect focal ERG responses from graft tissues may have been partly due to small graft size or programming of focal ERGs to detect only cone

function. Increasing the size or number of grafts to improve the overall chance of direct integration—in addition to improving experimental protocols to detect focal rod function—represents a future challenge. The use of previously reported environmental factors, including chondroitinase ABC or valproic acid, may increase the chance of graft integration (38). Because the presence of graft inner cells is a known major cause of host–graft integration failure, the customization of differentiation conditions toward the photoreceptor lineage rather than inner cells may be useful.

Although this was an introductory study of hESC-retina transplantation using primate models, we were able to characterize the maturation process of hESC-retinas in detail after xenotransplantation with immune suppression. The results of the present study demonstrate the potential utility of these models in further studies of graft optimization or surgical conditions. Further, the present study demonstrates a method of monitoring graft status in vivo by using clinically relevant examinations, including OCT and focal ERG, and a number of subjective examinations including VA tests and in an animal-friendly manner. These methods may also facilitate greater understanding and further insights from human studies.

Materials and Methods

Retinal Differentiation of hESCs and Graft Preparation. Human ESCs (KhES-1) were used according to the hESC research guidelines of the Japanese government. The use of hESC reporter lines (Rx::Venus and Crx::Venus) has been described (15). hESCs were maintained and differentiated as described (16). In brief, hESCs were maintained on mitotically inactivated MEFs in DMEM/F12 supplemented with 20% (vol/vol) knockout serum replacement (KSR; Gibco, Thermo Fisher Scientific), 2 mM glutamine, 0.1 mM nonessential amino acids (Gibco), 7.5 ng/mL recombinant human basic FGF (Wako), 0.1 mM 2-mercaptoethanol, 50 U/mL penicillin, and 50 μg/mL streptomycin (P/S). For retinal differentiation by serum-free floating culture of embryoid body-like aggregates with quick reaggregation (SFEBq) culture, hESCs were dissociated into single cells in TrypLE Express (Gibco) containing 0.05 mg/mL DNase I (Roche) and 20 μM Y-27632 before quick reaggregation using low-cell-adhesion 96-well plates with V-bottomed conical wells (Sumitomo Bakelite) in "differentiation medium" (12,000 cells per well, 100 μL), supplemented with 20 μM Y-27632. Differentiation medium comprised growth factor-free CDM (gfCDM) containing 45% Iscove's modified Dulbecco's medium (Gibco), 45% F12 (Gibco), Glutamax, 10% KSR, 1% chemically defined lipid concentrate (Gibco), and monothioglycerol (450 μM; Sigma). Defining the day on which the SFEBq culture was started as DD0, recombinant human BMP4 (R&D) was added to culture to a final concentration of 1.5 nM on DD6, and its concentration was diluted half by half by medium change every third day. At DD18, aggregates forming retinal tissue were transferred to a 9-cm Petri dish (noncell adhesive; Sumitomo Bakelite) and further cultured in suspension for 4–6 d in DMEM/F12-Glutamax medium (Gibco) containing 1% N_2 supplement, 3 μM CHIR99021 (GSK3 inhibitor; Stemgent), and 5 μM SU5402 (FGFR inhibitor; Sigma). To induce neural retina (NR) tissue, floating aggregates with RPE-like thin epithelium were then cultured in suspension in NR-differentiation medium containing DMEM/F12-Glutamax medium (Gibco), 1% N_2 supplement (Gibco), 10% FBS, 0.5 μM retinoic acid (Sigma), 0.1 mM taurine (Sigma), Fungizone, and P/S.

For graft preparation, transparent and continuous NR tissue epithelium was cut into 0.5-mm-wide sheets by using a microknife. Grafts were kept in HBSS buffer on ice for <2 h before transplantation.

Transplantation into Nude Rats. In all of the animal experiments, animals were treated in accordance with the Association for Research in Vision and Ophthalmology statement for the use of Animals in Ophthalmic and Vision Research. All animal experiments in this study were conducted with the approval of the Animal Research Committee at RIKEN Center for Developmental Biology institute. Animals were sedated with a mixture of ketamine and xylazine, pupils were dilated with 0.5% tropicamide and 0.5% phenylephrine hydrochloride, and corneas were anesthetized with topical 1% tetracaine when needed. The procedures about transplantation into nude rats are described fully in *SI Materials and Methods*.

Monkey Models. A total of eight monkeys (M1 to M8) were used for the experiments, and the types of injury induced and in vivo examinations performed in each monkey eye are summarized in Table S2. The monkeys used in this study were either provided by Shin Nippon Biomedical Laboratories or obtained from Japan Bio Science Center. Seven adult cynomolgus monkeys (*Macaca fascicularis*) and a rhesus monkey (*Macaca mulatta*) were used, each weighing 4–6 kg and aged between 4 and 11 y at the time of intervention. Monkeys were treated with either subretinal injection of cobalt chloride or laser photocoagulation under anesthesia.

Cobalt chloride hexahydrate (Nacalai tesque) was dissolved in 0.9% saline solution. For practical reasons, we conventionally defined the concentrations as of cobalt chloride hexahydrate used ($CoCl_2{\cdot}6H_2O$, molecular weight of 237.93). Cobalt chloride hexahydrate solution of 0.20, 0.25, 0.30, and 0.40 mg/mL was prepared for injury induction. Localized retinal detachments were created by subretinal injection of 40 μL of cobalt chloride solution using a cannula (rigid injection cannula; Synergetics). For laser injury, the 577-nm OPSL PASCAL laser system (Topcon Medical Laser Systems) was applied. By using modified computer software, laser size was fixed at 100 μm with a pulse duration of 15 ms. Approximately 25 spots (5 vertical × 5 horizontal) were applied almost simultaneously by using single foot pedal depression. Intervals between spots were set at 0 μm. A standard retinal laser contact lens (QuadrAspheric; Volk) was used to focus lasers onto monkey fundus. The magnification of the used contact lens was ×1.97. Before laser treatment, trial photocoagulation in adjacent areas was performed by using a range of laser powers from 110 to 175 mW, and the powers were adjusted in accordance with the degree of retinal degeneration. To induce selective ONL damage, we first aimed to induce "barely visible" grade photocoagulation (37). Lesions were then evaluated by direct fundus observation and by OCT imaging within 5 min after treatment. Where lesions were intermittently induced between adjoining spots, the laser power was increased to achieve heat diffusion into neighboring regions to an extent that did not affect INL. After the power was determined, continuous regions were injured with laser treatment.

Transplantation into Monkey Models. Transplantation of hESC-retinas was performed in four eyes of three monkeys at 98, 109, 77, and 46 d after induction of retinal degeneration (one laser model and three eyes of cobalt model, M1–M3; Table S2). The procedures about transplantation into monkey models are described fully in *SI Materials and Methods*.

In Vivo Examinations After Injury Induction and Transplantation. In vivo examinations performed in each monkey are summarized in Table S2. During the observation period, all of the eyes were monitored by using a fundus camera (CX-1, Canon; RetCam, Clarity) with or without an FA barrier filter and with OCT (RS3000; Nidek) at 3 or 4 d, 2 wk, and every month following procedures. Minimal ONL thickness of the central lesion at the injury sight was measured at 1 and 2 wk and 1 and 2 mo after procedure in the same section as evaluated by OCT. Focal ERG recordings were conducted at 2 wk and every month after treatment. Two monkeys (M1 and M2) were trained to perform VA tests.

Focal ERG Recording. The Burian–Allen bipolar contact lens electrode (Hansen Ophthalmic Laboratories) was attached, and a ground electrode was placed on the ear. An ER-80 (Kowa) was used to elicit focal ERGs. Band-pass filters were set at 5–500 Hz. The spot size was at 15°. The stimulus repetition rate was 2 Hz, and 200 responses were averaged (MEB-9402 Neuropack; Nihon Kohden).

VA Testing. Monkeys were first trained to distinguish one box labeled with a Landolt ring (unlocked) from the five other boxes labeled with continuous rings (locked) in a stress-free environment by rewarding upon opening the lid of the unlocked, correct box. The "correct response" was only judged on the first attempt by the monkey to open any lid; otherwise, no reward was given (Movie S1). Well-trained monkeys were then placed in a test cage with a line of small peeking holes along the edge of two walls to conduct the same task using monocular vision (Fig. S4*A*, arrows and arrowheads). Peeking holes and labeled plates were placed in such a way that monkeys were only able to see a plate through a hole with one eye closer to the wall end (Fig. S4 *B–D*). Monkeys were required to select and open the one box with a Landolt ring out of a total of three boxes, with the other two boxes having continuous rings (Fig. S4*E*). The arrangement of the Landolt or continuous rings and the direction of the break in the Landolt ring were determined by using a table of random numbers. Every care was taken to avoid disclosing the examiner's intention; label rearrangement was predominantly performed while monkeys were not paying attention, and the examiner pretended to turn the screw or lock the lid of the box with a Landolt ring (unlocked) (Movies S2 and S3). VA was calculated according to the size of, and the distance to, a Landolt ring. Trained monkeys obtained a maximal VA of logMAR 0.7, with a constant success rate of >90%. A score of >75% in

20 trials was judged as a "pass," whereas lower scores were judged as a "failure." In cases of scores <50% in the first seven trials with any VA, monkeys were tested with a larger ring, or a poorer VA, in a stepwise manner. The VA of opposite eyes was also tested on the same day as a positive control to evaluate the condition of monkeys regarding their ability to perform the task.

Immunohistological Procedures. The procedures used for immunohistological analyses are described fully in *SI Materials and Methods*.

Histological Analyses. For the evaluation of the cobalt and laser models, at least four different sections of lesional areas were examined by hematoxylin and eosin and immunohistochemical analyses. Normal regions of the same injured eyes were used as positive controls.

For nude rat transplantation studies, ONL thickness of grafts was measured as the average number of photoreceptor nuclei at four locations in vertical and horizontal directions of each rosette. Three or four different fields of ~100 μm apart to avoid overlaps of rosettes were observed per each eye, and the three thickest rosettes in each field were counted for ONL thickness; if there were fewer than three rosettes in a field, ONL thickness of all of the rosettes was measured. In nude rats with retinal degeneration, ONL thickness was measured in all of the rosettes in a 50-μm section per eye. The proportion of cells positive for cone opsins was calculated from three cone-positive rosettes in three or four different fields for each sample. The proportion of directly integrated graft rosettes in retinal degenerative nude rats was calculated from at least two sections of 50-μm thickness in which substantial regions of grafted cells were observed in the subretinal space of host retinas. In cases where dendrites of host bipolar cells were observed in contact with graft photoreceptors or ONL of rosettes on 3D immunohistochemical imaging, rosettes were judged to be directly integrated into host retinas. The number of rosettes observed to have directly integrated with host bipolar cells was divided by the number of rosettes adjacent to host INL with or without graft inner cells for each eye. Counting was performed by a single investigator in a blind manner.

For grafts in monkey models, $Ki67^+$ cells were counted in three sections, including one section from the middle of the graft-containing area and two evenly spaced sections within the graft area. Three rosettes were randomly selected per section, and the proportion of Ki67 and DAPI dual-positive cells in each rosette was calculated and averaged for each eye. The proportion of cone $opsin^+$ cells was counted in an identical manner, but including cone $opsin^+$ rosettes only.

The number of rosettes expressing each of the photoreceptor markers recoverin, rhodopsin, and cone opsin was counted individually in three sections, including one section from the middle of the graft-containing area and two evenly spaced sections within the graft area. The proportion of positive rosettes was calculated as the total number of positive rosettes for each marker divided by the total number of rosettes in the same three sections for each eye (mostly >10 rosettes were detected in total per each section). Positivity was judged as complete when photoreceptor markers were observed evenly throughout rosette structures and judged as partial otherwise.

Electron Microscopy. The procedures used for electron microscopy analysis are described fully in *SI Materials and Methods*.

Statistics. Statistical significance was assessed by using analysis of variance (ANOVA) with Bonferroni's correction or Student–Newman–Keuls test where indicated.

ACKNOWLEDGMENTS. We thank Tomoyo Hashiguchi for technical support; Wataru Ohashi and Masayuki Kawahara for technical assistance in animal experiments; Shin Nippon Biomedical Laboratories, Ltd., for providing monkeys; Genshiro Sunagawa for advice on statistics; and members of the M.T. laboratory for discussions. This study was supported by a grant from the Research Center Network for Realization of Regenerative Medicine, Japan Agency for Medical Research and Development.

1. Hartong DT, Berson EL, Dryja TP (2006) Retinitis pigmentosa. *Lancet* 368(9549): 1795–1809.
2. Punzo C, Kornacker K, Cepko CL (2009) Stimulation of the insulin/mTOR pathway delays cone death in a mouse model of retinitis pigmentosa. *Nat Neurosci* 12(1):44–52.
3. Berson EL, et al. (1993) A randomized trial of vitamin A and vitamin E supplementation for retinitis pigmentosa. *Arch Ophthalmol* 111(6):761–772.
4. Berson EL, et al. (2004) Further evaluation of docosahexaenoic acid in patients with retinitis pigmentosa receiving vitamin A treatment: Subgroup analyses. *Arch Ophthalmol* 122(9):1306–1314.
5. Jacobson SG, et al. (2012) Gene therapy for leber congenital amaurosis caused by RPE65 mutations: Safety and efficacy in 15 children and adults followed up to 3 years. *Arch Ophthalmol* 130(1):9–24.
6. Humayun MS, et al.; Argus II Study Group (2012) Interim results from the international trial of Second Sight's visual prosthesis. *Ophthalmology* 119(4):779–788.
7. Doroudchi MM, et al. (2011) Virally delivered channelrhodopsin-2 safely and effectively restores visual function in multiple mouse models of blindness. *Mol Ther* 19(7): 1220–1229.
8. Gaub BM, et al. (2014) Restoration of visual function by expression of a light-gated mammalian ion channel in retinal ganglion cells or ON-bipolar cells. *Proc Natl Acad Sci USA* 111(51):E5574–E5583.
9. MacLaren RE, et al. (2006) Retinal repair by transplantation of photoreceptor precursors. *Nature* 444(7116):203–207.
10. Lamba DA, Gust J, Reh TA (2009) Transplantation of human embryonic stem cell-derived photoreceptors restores some visual function in Crx-deficient mice. *Cell Stem Cell* 4(1):73–79.
11. Pearson RA, et al. (2012) Restoration of vision after transplantation of photoreceptors. *Nature* 485(7396):99–103.
12. Gonzalez-Cordero A, et al. (2013) Photoreceptor precursors derived from three-dimensional embryonic stem cell cultures integrate and mature within adult degenerate retina. *Nat Biotechnol* 31(8):741–747.
13. Seiler MJ, Aramant RB (2012) Cell replacement and visual restoration by retinal sheet transplants. *Prog Retin Eye Res* 31(6):661–687.
14. Assawachananont J, et al. (2014) Transplantation of embryonic and induced pluripotent stem cell-derived 3D retinal sheets into retinal degenerative mice. *Stem Cell Rep* 2(5):662–674.
15. Nakano T, et al. (2012) Self-formation of optic cups and storable stratified neural retina from human ESCs. *Cell Stem Cell* 10(6):771–785.
16. Kuwahara A, et al. (2015) Generation of a ciliary margin-like stem cell niche from self-organizing human retinal tissue. *Nat Commun* 6:6286.
17. Zhong X, et al. (2014) Generation of three-dimensional retinal tissue with functional photoreceptors from human iPSCs. *Nat Commun* 5:4047.
18. Seiler MJ, et al. (2014) A new immunodeficient pigmented retinal degenerate rat strain to study transplantation of human cells without immunosuppression. *Graefes Arch Clin Exp Ophthalmol* 252(7):1079–1092.
19. Hara A, et al. (2006) A new model of retinal photoreceptor cell degeneration induced by a chemical hypoxia-mimicking agent, cobalt chloride. *Brain Res* 1109(1):192–200.
20. Murakami I, Komatsu H, Kinoshita M (1997) Perceptual filling-in at the scotoma following a monocular retinal lesion in the monkey. *Vis Neurosci* 14(1):89–101.
21. Schmitz F, Königstorfer A, Südhof TC (2000) RIBEYE, a component of synaptic ribbons: A protein's journey through evolution provides insight into synaptic ribbon function. *Neuron* 28(3):857–872.
22. Noell WK (1952) The impairment of visual cell structure by iodoacetate. *J Cell Physiol* 40(1):25–55.
23. Fuller D, Machemer R, Knighton RW (1978) Retinal damage produced by intraocular fiber optic light. *Am J Ophthalmol* 85(4):519–537.
24. Strazzeri JM, et al. (2014) Focal damage to macaque photoreceptors produces persistent visual loss. *Exp Eye Res* 119:88–96.
25. Vengellur A, LaPres JJ (2004) The role of hypoxia inducible factor 1alpha in cobalt chloride induced cell death in mouse embryonic fibroblasts. *Toxicol Sci* 82(2):638–646.
26. Yu DY, Cringle SJ (2005) Retinal degeneration and local oxygen metabolism. *Exp Eye Res* 80(6):745–751.
27. Humayun MS, et al. (2000) Human neural retinal transplantation. *Invest Ophthalmol Vis Sci* 41(10):3100–3106.
28. Radtke ND, Aramant RB, Seiler M, Petry HM (1999) Preliminary report: Indications of improved visual function after retinal sheet transplantation in retinitis pigmentosa patients. *Am J Ophthalmol* 128(3):384–387.
29. Radtke ND, et al. (2008) Vision improvement in retinal degeneration patients by implantation of retina together with retinal pigment epithelium. *Am J Ophthalmol* 146(2):172–182.
30. West EL, et al. (2010) Long-term survival of photoreceptors transplanted into the adult murine neural retina requires immune modulation. *Stem Cells* 28(11):1997–2007.
31. Strettoi E, Pignatelli V (2000) Modifications of retinal neurons in a mouse model of retinitis pigmentosa. *Proc Natl Acad Sci USA* 97(20):11020–11025.
32. Cuenca N, et al. (2004) Regressive and reactive changes in the connectivity patterns of rod and cone pathways of P23H transgenic rat retina. *Neuroscience* 127(2):301–317.
33. Liets LC, Eliasieh K, van der List DA, Chalupa LM (2006) Dendrites of rod bipolar cells sprout in normal aging retina. *Proc Natl Acad Sci USA* 103(32):12156–12160.
34. Eliasieh K, Liets LC, Chalupa LM (2007) Cellular reorganization in the human retina during normal aging. *Invest Ophthalmol Vis Sci* 48(6):2824–2830.
35. Samuel MA, et al. (2014) LKB1 and AMPK regulate synaptic remodeling in old age. *Nat Neurosci* 17(9):1190–1197.
36. Sher A, et al. (2013) Restoration of retinal structure and function after selective photocoagulation. *J Neurosci* 33(16):6800–6808.
37. Paulus YM, et al. (2008) Healing of retinal photocoagulation lesions. *Invest Ophthalmol Vis Sci* 49(12):5540–5545.
38. Mandai M, et al. (2012) Adequate time window and environmental factors supporting retinal graft cell Survival in rd mice. *Cell Med* 4(1):45–54.
39. Kamao H, et al. (2014) Characterization of human induced pluripotent stem cell-derived retinal pigment epithelium cell sheets aiming for clinical application. *Stem Cell Rep* 2(2):205–218.